PAPER

Tantalum(v) 1,3-propanediolate β-diketonate solution as a precursor to sol–gel derived, metal oxide thin films†

Christopher Beale, [ab] Stefanie Hamacher, [ab] Alexey Yakushenko, [c] Oumaima Bensaid, [ab] Sabine Willbold, [d] Guillermo Beltramo, [e] Sören Möller, [f] Heinrich Hartmann, [d] Elmar Neumann, [g] Gregor Mussler, [h] Alexander Shkurmanov, [h] Dirk Mayer, [a] Bernhard Wolfrum [ai] and Andreas Offenhäusser [*a]

Tantalum oxide is ubiquitous in everyday life, from capacitors in electronics to ion conductors for electrochromic windows and electrochemical storage devices. Investigations into sol–gel deposition of tantalum oxide, and its sister niobium oxide, has accelerated since the 1980s and continues to this day. The aim of this study is to synthesize a near UV sensitive, air stable, and low toxicity tantalum sol–gel precursor solution for metal oxide thin films – these attributes promise to reduce manufacturing costs and allow for facile mass production. By utilizing 1D and 2D nuclear magnetic resonance, this study shows that by removing ethanol from the precursor solution at a relatively low temperature and pressure, decomposition of the photosensitive complex can be minimized while obtaining a precursor solution with sufficient stability for storage and processing in the atmosphere. The solution described herein is further modified for inkjet printing, where multiple material characterization techniques demonstrate that the solution can be utilized in low temperature, photochemical solution deposition of tantalum oxide, which is likely amorphous. Tested substrates include amorphous silica, crystalline silicon wafer, and gold/titanium/PET foil. The hope is that these results may spark future investigations into electronic, optical, and biomedical device fabrication with tantalum oxide, and potentially niobium oxide, based films using the proposed synthesis method.

Introduction

At the start of World War II, Lieutenant Commander O. Hugh Fulcher of the United States Navy performed the first successful cranioplasty with tantalum metal, claiming it as the most suitable material and as to "keep as many men at as many guns as many days as possible".[1] The success of tantalum in medical

[a] IBI-3, Bioelectronics, Forschungszentrum Jülich GmbH, D-52425, Germany. E-mail: a.offenhaeusser@fz-juelich.de

[b] RWTH Aachen University, Templergraben 55, D-52062, Germany

[c] Fraunhofer Research Institute for Microsystems and Solid State Techologies, D-80686 Munich, Germany

[d] ZEA-3, Analytics, Forschungszentrum Jülich GmbH, D-52425, Germany

[e] IBI-2, Mechanobiology, Forschungszentrum Jülich GmbH, D-52425, Germany

[f] IEK-1, Materials Synthesis and Processing, Forschungszentrum Jülich GmbH, D-52425, Germany

[g] Helmholtz Nano Facility, Forschungszentrum Jülich GmbH, D-52425, Germany

[h] PGI-9, Semiconductor Nanoelectronics, Forschungszentrum Jülich GmbH, D-52425, Germany

[i] Neuroelectronics, Munich School of Bioengineering, Department of Electrical and Computer Engineering, Technical University of Munich (TUM), D-85748 Garching, Germany

† Electronic supplementary information (ESI) available. See DOI: 10.1039/d0ra02558e

implants was known to be due to a biocompatible, corrosion resistant oxide film which forms on the surface of the metal.[2] Modern medical research has additionally elucidated that implants having a porous tantalum coating upregulate osteogenic genes, resulting in greater osteointegration when compared to titanium implants without the coating.[3] Aside from applications in orthopedic implants,[4] tantalum and its sister niobium form oxides which have a variety of uses, including capacitors,[5] batteries,[6,7] electrochromic windows,[8] pH and conductivity sensors,[9–13] surface plasmon resonance sensors,[14–16] ferroelectric memory devices,[17–20] corrosion resistant coatings,[21] and even gravity wave detectors.[22]

During manufacturing of such devices, production inefficiencies and waste material lead to the addition of a recycling step,[23] thereby complicating the fabrication of products containing tantalum. Efforts to deposit such oxides *via* additive processes at relatively low temperatures, which would save material and energy,[24–26] still remain a challenge. Therefore, this study aims to further investigations into additive processing *via* inkjet printing and low temperature annealing of tantalum oxide, and potentially niobium oxide, with a focus on the sol–gel method – this method is a subset of chemical solution deposition (CSD) and photochemical solution deposition (PCSD). Advantages of the sol–gel method include lower costs,

stoichiometry control, and feasible implementation into a roll-to-roll manufacturing line.[27,28]

## Sol–gel synthesis with niobium and tantalum alkoxides

In order to produce metal oxide films free of halide impurities *via* the sol–gel route, a metal halide precursor can be converted to a metal alkoxide derivative before use in CSD or PCSD.[29] Avoiding halides may also be necessary in some cases, while compounds such as hydrochloric acid can be formed during synthesis, thus creating an acidic environment which may be undesirable.[30] However, niobium and tantalum alkoxides (dimers at room temperature) are relatively sensitive to atmospheric moisture *via* the following reaction[31–34] (M = Nb, Ta; R = methyl, ethyl):

$$M_2(OR)_{10} + 5H_2O \rightarrow M_2O_5 + 10ROH \tag{1}$$
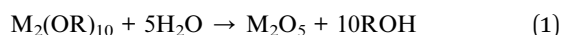
An option to minimize hydrolysis from water is by using 2-methoxyethanol as the solvent for the metal alkoxide precursor, due to 2-methoxyethanol's ability to prevent nucleophilic attack from water to the cation *via* a chelate complex.[35] Although 2-methoxyethanol is often used as a solvent in CSD,[36] 2-methoxyethanol has been reported to have developmental and reproductive toxicity,[35] and poses a danger *via* inhalation (with its relatively high vapor pressure) and skin exposure. Furthermore, in light of its inherent toxicity, use of 2-methoxyethanol has been restricted in some countries, thus making its use in manufacturing difficult.[35] This calls for alternative strategies to prevent hydrolysis before solution deposition.

Sol–gel synthesis with glycolate solutions

One way to avoid 2-methoxyethanol is by using glycols as a solvent instead. Following the work of Mehrotra and Kapoor[37,38] in 1965, where glycol substitution in niobium and tantalum ethoxides was described, Calzada and González[17,18] reported in 2005 the substitution of ethoxy groups in tantalum(v) ethoxide with 1,3-propanediol *via* reflux and distillation. This resulted in a tantalum(v) 1,3-propanediolate solution, which is air stable for months:

$$Ta(OC_2H_5)_5 + 5HOC_3H_6OH \rightarrow Ta(OC_3H_6OH)_5 + 5C_2H_5OH \tag{2}$$
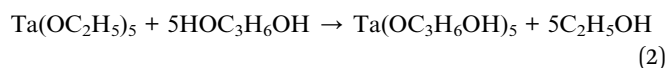
In this case, the substituting glycol also acts as the solvent, which simplifies the formulation of the solution. 1,3-Propanediol has also been used for niobium based solutions.[19,20]

The air stable, low toxic tantalum(v) 1,3-propanediolate solution produced by Calzada and González proves advantageous for high temperature CSD,[17,18] and possibly even for far UV processing in PCSD where exposure of tantalum(v) ethoxide to these conditions has resulted in tantalum oxide films.[39,40] However, the solution is likely not suitable for low temperature and near UV processing as its photoabsorption in this range would likely be too low.[39,40]

Sol–gel synthesis with β-diketonate complexes

One way to increase the photoabsorption for near UV processing is to chelate a β-diketone or β-ketoester to the metal cation.[41–45] These ligands can absorb in the 200 nm to 380 nm range as a result of the π → π* transition (*i.e.*, the π bonding to π antibonding transition), where photo-excitation can result in ligand dissociation and metal oxide formation,[26,35,41] with the photochemical mechanism described in detail by Segawa *et al.*[46] and Squibb *et al.*[47]

After Whitley[48,49] pioneered the synthesis of various tantalum(v) alkoxides for her PhD thesis in 1954 by following the experiments of Funk and Niederländer,[50,51] she reported in her same work the chelation of benzoylacetone to an ethoxide of tantalum.[48,52] This was later confirmed for various β-diketonate and β-ketoester compounds with niobium and tantalum[53–56] (M = Nb, Ta; R = methyl, ethyl; AH = β-diketone or β-ketoester; A = chelated form; x = 1–3):

$$M(OR)_5 + xAH \rightarrow (RO)_{5-x}MA_x + xROH \tag{3}$$
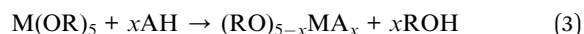
Glycolate solutions with β-diketonate complexes

When mixing metal β-diketonate complexes with glycols, preliminary attempts at isolating metal glycolate β-diketonate complexes were reported in the 1990s. For example, Calzada and coworkers[57] claim to have successfully produced titanium(iv) 1,3-propanediolate bis acetylacetonate complexes *via* reflux and discuss their potential use in PCSD.[58]

However, Kemmitt and Daglish[59] found that prolonged solution exposure to heat leads to the alcoholysis of acetylacetone and the acetylation of 1,3-propanediol, resulting in the decomposition of the titanium(iv) acetylacetonate complex and the formation of an insoluble $Ti(iv)(OC_3H_6O)_2$ precipitate (both terminal oxygens being bound to the Ti(iv) cation). This indicates that attempts at creating metal glycolate β-diketonate solutions may result in unwanted side products, thus decreasing the amount of desired β-diketonate complexes, which are necessary for photosensitivity in the near UV range. Alcoholysis of other metal acetylacetonates, resulting in acetylation of alcohol groups for nanoparticle formation,[60,61] has been known for some time.[62]

Thus, in order to combine the benefits of tantalum or niobium glycolate solutions, those being low toxicity and stability in ambient conditions, with the near UV photosensitivity of tantalum or niobium β-diketonate complexes, a procedure is needed which reduces the chance of complex alcoholysis when mixing glycols, such as 1,3-propanediol, with niobium or tantalum β-diketonate complexes. This would lead not only to safer, stable solutions that could be more easily used in manufacturing facilities, but would also result in a more efficient β-diketone chelation reaction while minimizing the formation of side products from alcoholysis.

Therefore, this study will characterize two solutions from a proposed synthesis method *via* nuclear magnetic resonance (NMR), where 1,3-propanediol is added to an ethanol solution containing tantalum(v) acetylacetonate or tantalum(v) benzoylacetonate complexes at a reduced temperature with subsequent ethanol removal at a reduced pressure, with the desired reaction (A = chelated β-diketone):

$$TaA(OC_2H_5)_4 + 4HOC_3H_6OH \rightarrow TaA(OC_3H_6OH)_4 + 4C_2H_5OH \tag{4}$$
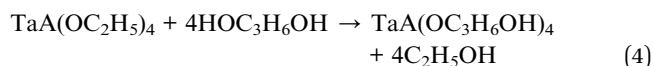
Solution synthesis characterization will be followed by examination of the tantalum oxide layers derived from these solutions.

Results and discussion

In preparing the tantalum(v) ethoxide β-diketonate precursor, anhydrous ethanol was chosen as the reflux solvent since lighter monoalcohols are less likely to undergo alcoholysis than heavier diols in the presence of a metal cation and a β-diketone.[59] In support of this, exposure of the Calzada and González tantalum(v) 1,3-propanediolate precursor[18] with acetylacetone to <80 °C over 72 hours demonstrates that alcoholysis with 1,3-propanediol is possible in the absence of ethanol (see ESI†). Therefore, higher temperatures with heavier diols should be avoided, as well as long reflux times with lighter monoalcohols where 8 hours should be sufficient.[48,55,63] Reflux solvents such as benzene[48,55] or tetrahydrofuran[63] could be used, but the former is carcinogenic and the latter may present an explosion hazard.

Proposed synthesis method

The proposed method for minimizing alcoholysis from 1,3-propanediol first involves acquiring or forming a tantalum(v) ethoxide β-diketonate complex, followed by mixing the complex with 1,3-propanediol at room temperature (rather than under reflux[17,18,57,59]). The mixing should lead to the substitution of the ethoxide groups with 1,3-propanediol, where the reaction is driven to completion by adjusting the system temperature and pressure so that ethanol distills without 1,3-propanediol also distilling or causing decomposition of the tantalum(v) β-diketonate complex.

More particularly, the distillation temperature and pressure should be chosen such that alcoholysis of the tantalum(v) β-diketonate complex is minimized and that the vapor pressure of ethanol is greater than the pressure of the closed system, while the vapor pressure of 1,3-propanediol and the tantalum(v) 1,3-propanediolate β-diketonate complex is less than the pressure of the closed system. After ethanol removal, the tantalum(v) 1,3-propanediolate β-diketonate solution would be isolated in a liquid form at room temperature, ready for CSD or PCSD.

For example in Fig. S1,† at 23 °C ethanol has a vapor pressure of 70 mbar,[64,65] while 1,3-propanediol has a vapor pressure of 0.1 mbar[66,67] (1,3-propanediol data are extrapolated beyond the experimental data range *via* the literature Antoine parameters). By increasing the temperature mildly to 40 °C, ethanol's vapor pressure increases to 180 mbar[64,65] and 1,3-propanediol's to 0.4 mbar[66,67] (the latter still being a theoretical extrapolation). Thus, at 40 °C the system pressure should be set above 0.4 mbar and below 180 mbar in order to remove ethanol from the solution, which should then allow the tantalum(v) 1,3-propanediolate β-diketonate solution to remain.

Therefore, when starting with 1,3-propanediol and a tantalum(v) tetraethoxide β-diketonate complex, such as tantalum(v) tetraethoxide acetylacetonate or tantalum(v) tetraethoxide benzoylacetonate, under the optimal temperature and pressure the desired substitution may proceed as shown in Fig. 1. If the
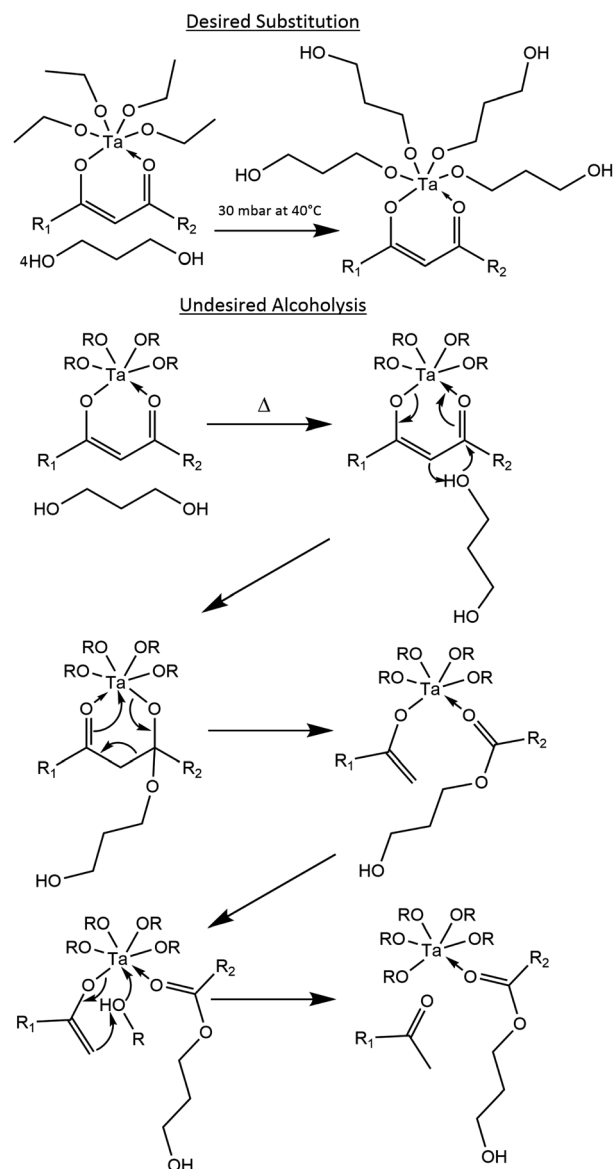

Fig. 1 Desired substitution of ethanol with 1,3-propanediol, and the undesired mechanism of alcoholysis; acetylacetone: $R_1 = R_2 = $ methyl; benzoylacetone: $R_1 \neq R_2$, $R_1 = $ methyl or phenyl, $R_2 = $ methyl or phenyl.

temperature is set too high and for too long, then undesired alcoholysis of the complex is more likely, with the proposed reaction mechanism[62] also shown in Fig. 1.

After removing the ethanol at 30 mbar and <40 °C in both the acetylacetone and the bezoylacetone solutions over 8 hours, the benzoylacetone solution from the proposed method in Fig. 2b appears to be redshifted from that of the acetylacetone solution in Fig. 2a. Furthermore, no visible, insoluble precipitates are present, as was reported for Ti(iv) and Zr(iv) acetylacetonate complexes in the presence of 1,3-propanediol (where $M(IV)(OC_3H_6O)_2$ was formed).[59] Additionally, when Ta(v) ethoxide is replaced with Ti(iv) isopropoxide, a turbid solution forms at room temperature after 1,3-propanediol addition (see ESI†). The lack of visible precipitates in the Ta(v) solutions may
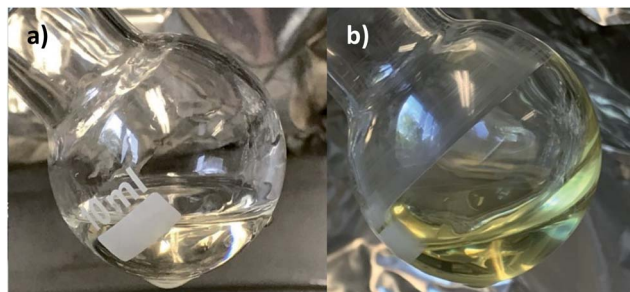
Fig. 2 Final solution products from the proposed method with acetylacetone (a), and the proposed method with benzoylacetone (b), where (b) appears redshifted relative to (a).

be due to the odd, +5 valency of the cation. UV/Vis spectrophotometry for the solutions was not performed, as this would require a significant dilution, thereby changing the product. Therefore, UV/Vis absorption of the printed layers was performed instead (described later), which is more relevant for applications in PCSD.

NMR measurements

^{1}H and ^{13}C NMR spectra of the reagents are shown in Fig. S2–S9,† which aided in the peak assignments described in this section. Total correlation spectroscopy (TOCSY) and heteronuclear multiple bond correlation (HMBC) spectra were also used to assign peaks for some of the products. Fig. 3 serves as a visual aid for the discussion.

NMR: proposed synthesis – acetylacetone

The ^{1}H NMR spectrum of the product (δ [ppm], Fig. S10 and S11†) shows the presence of the expected 1,3-propanediol peaks at δ 1.81 [HOCH$_2$CH_2CH$_2$OH], δ 3.72 [HOCH_2CH$_2$CH_2OH], and δ 5.21 [HOCH$_2$CH$_2$CH$_2$OH]. Three separate methine acetylacetone-enol peaks appear at δ 5.96, δ 5.87, and δ 5.74 [H$_3$C(CO)CH(CO)CH$_3$]. The peaks from δ 2.30 to δ 2.14 overlap significantly (with δ 2.21 being the most prominent peak, see Fig. S11†), making the following methyl peak assignments

Fig. 3 Reference structures with NMR data in the ESI† and literature. In the β-diketone enol tautomer, the upper proton can be replaced by a metal cation; acetylacetone: R$_1$ = R$_2$ = methyl; benzoylacetone: R$_1$ ≠ R$_2$, R$_1$ = methyl or phenyl, R$_2$ = methyl or phenyl.

tentative: acetylacetone-keto [H$_3$C(CO)CH$_2$(CO)CH$_3$] or acetone [H$_3$C(CO)CH_3] methyl peaks (the latter from alcoholysis)[59,68] occur at δ 2.30 and δ 2.26, and the acetylacetone-enol [H$_3$C(CO) CH(CO)CH_3] methyl peaks around δ 2.21 and δ 2.14. The multiple peaks for the same proton on the acetylacetone-enol tautomer may be due to the different ways in which acetylacetone can bind to the metal cation.[62]

Further downfield, as the δ 4.21 peak resonates at a higher frequency than the alcoholic methylene 1,3-propanediol peak at δ 3.72, in addition to the presence of another overlapping methyl peak at δ 2.14, likely indicates the acetylation of 1,3-propanediol and the creation of 3-hydroxypropyl acetate,[69] despite the extra steps taken to avoid alcoholysis of the complex. One of the overlapping peaks at δ 2.14 would then correspond to the methyl attached to the ester carbonyl [HOCH$_2$CH$_2$CH$_2$-O(CO)CH_3], and the peak at δ 4.21 would be the protons on the methylene carbon bound to the ester oxygen [HOCH$_2$CH$_2$CH_2-O(CO)CH$_3$]. Additionally, the TOCSY spectrum in Fig. S12† shows three distinct proton groups on three consecutive carbon atoms, and the ^{13}C NMR and HMBC spectra corroborate these findings (discussed next), as well as the literature values for 3-hydroxypropyl acetate.[70] It is not clear whether the δ 4.21 peak occurs as a triplet, and the peak at δ 4.65 is difficult to assign with the available data.

The ^{13}C NMR spectrum of the product (δ [ppm], Fig. S13†) shows the expected 1,3-propanediol peaks at δ 35.2 [HOCH$_2$-CH$_2$CH$_2$OH] and δ 59.0 [HOCH$_2$CH$_2$CH$_2$OH]. Acetylacetone-enol peaks around δ 192.0 [H$_3$C(CO)CH(CO)CH$_3$], around δ 102.0 [H$_3$C(CO)CH(CO)CH$_3$], and around δ 26.2 [H$_3$$C$(CO) CH(CO)$CH_3$] appear in the spectrum, along with some acetylacetone-keto [H$_3$C(CO)CH$_2$(CO)CH$_3$] or acetone[59,71] [H$_3$C(CO)CH$_3$] peaks at δ 209.2 and δ 204.3, and around δ 31.6 [H$_3$$C$(CO)CH$_2$(CO)CH$_3$] or [H$_3$$C$(CO)CH$_3$]; there is possibly an acetylacetone-keto peak around δ 59.0 [H$_3$C(CO)CH$_2$(CO)CH$_3$], which is difficult to assign due to the presence of 1,3-propanediol. The peak at δ 171.8 [HOCH$_2$CH$_2$CH$_2$O(CO)CH$_3$], not associated with any of the reagents, is located in the range typically found for ester carbonyl carbons and would support the idea that 1,3-propanediol has been acetylated and that 3-hydroxypropyl acetate has been formed.[69] This is supported by literature[70] and the HMBC spectrum in Fig. S14,† which shows cross-peaks at ^{1}H δ 2.14–^{13}C δ 171.8 and ^{1}H δ 4.21–^{13}C δ 171.8. HMBC also shows no visible cross-peak at ^{1}H δ 4.65–^{13}C δ 171.8, possibly indicating that the compound with the ^{1}H δ 4.65 peak does not contain an acetylated alcohol.

NMR: proposed synthesis – benzoylacetone

The ^{1}H NMR spectrum of the product (δ [ppm], Fig. S15 and S16†) shows the presence of the expected 1,3-propanediol peaks at δ 1.68 [HOCH$_2$CH_2CH$_2$OH], δ 3.59 [HOCH_2CH$_2$CH_2OH], and δ 5.11 [HOCH$_2$CH$_2$CH$_2$OH]. Three separate methine benzoylacetone-enol peaks appear at δ 6.53, δ 6.44, and δ 6.24 (Ph = phenyl group) [Ph(CO)CH(CO)CH$_3$]. The peaks from δ 2.50 to δ 2.00 overlap significantly (with δ 2.22 being the most prominent peak), with the following tentative assignments: δ 2.46 for the benzoylacetone-keto methyl [Ph(CO)CH$_2$(CO)CH_3]
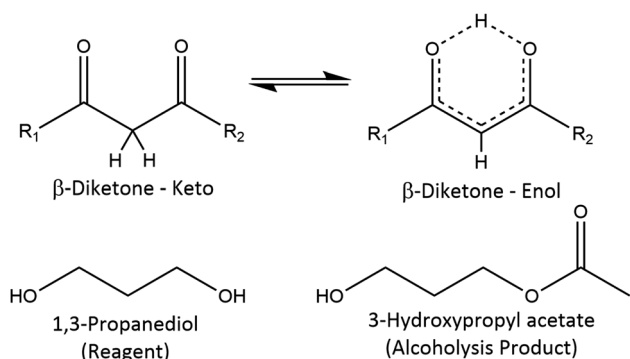
Paper

and around δ 2.22 for the enol methyl [PhC(CO)CH(CO)CH_3]. Peaks in the δ 8.00 to δ 7.30 range belong to the phenyl group protons on benzoylacetone [PhC(CO)CH(CO)CH$_3$]. Many unassigned peaks are present, possibly associated with different alcoholysis products. As for acetylacetone, benzoylacetone may be bound to the metal cation in different ways,[62] resulting in multiple peaks for the same proton.

The ^{13}C NMR spectrum of the product (δ [ppm], Fig. S17†) shows the expected 1,3-propanediol peaks at δ 35.1 [HOCH$_2$-CH$_2$CH$_2$OH] and δ 58.9 [HOCH$_2$CH$_2$CH$_2$OH]. Benzoylacetone-enol peaks around δ 193.0 [PhC(CO)CH(CO)CH$_3$], around δ 182.0 [PhC(CO)CH(CO)CH$_3$], around δ 100.0 [PhC(CO)CH(CO) CH$_3$], peak(s) within the range δ 28.0 to δ 25.0 [Ph(CO)CH(CO) CH$_3$] (difficult to assign exact peak), and the multiple phenyl ring carbon peaks (likely mixed in with those of the keto tautomer) in the range δ 140.0 to δ 125.0 [Ph(CO)CH(CO)CH$_3$] appear in the spectrum, along with some benzoylacetone-keto peaks at δ 199.2 [PhC(CO)CH$_2$(CO)CH$_3$], a carbonyl peak likely overshadowed by enol peaks in the range δ 195.0 to 190.0 [PhC(CO)CH$_2$(CO)CH$_3$], around δ 59.0 [H$_3$C(CO)CH$_2$(CO)CH$_3$] (difficult to assign exact peak), and peak(s) within the range δ 33.0 to δ 30.0 [Ph(CO)CH$_2$(CO)CH$_3$] (difficult to assign exact peak). The peak at δ 171.7, not associated with any of the reagents, is located in the range typically found for ester carbonyl carbons and would support the idea that acetylation of an alcohol group has occurred.[69]

Proposed synthesis product and ink rheology

For viscosity and surface tension measurements, separate syntheses of the proposed method (following the same procedures) were completed due to lack of material, and the reagent amounts are shown in Fig. S18.† Layers characterized by other methods described in this study were derived from the solutions which were produced for the NMR measurements.

Dilutions were made with diethylene glycol monoethyl ether (DEGEE), which allows the target viscosity ($\sim$10 mPa s) and surface tension ($\sim$30 mN m^{-1}) for inkjet printing to be reached. However, unlike how Matavž *et al.*[72] achieved the target viscosity and surface tension by mixing 1,3-propanediol with highly toxic 2-methoxyethanol, DEGEE presents a reduced exposure hazard with its lower vapor pressure, and can be used *in lieu* of 2-methoxyethanol to achieve the target values. The results are shown in Table 1.

UV/Vis – proposed synthesis method on a-SiO₂

For the acetylacetone based printed film, UV/Vis on a-SiO$_2$ in Fig. 4a and b shows a local maximum at 319 nm before xenon flash lamp exposure (125 °C anneal – 0 shots), demonstrating chelation of acetylacetone to the tantalum cation within the layer.[43,44] After firing 1000 shots on the layer, the peak at 319 nm disappears, and the global maximum redshifts to about 212 nm, which is similar to the maximum obtained in prior work *via* photoirradiation.[39,40] This shows that despite the solution impurities and alcoholysis byproducts that appear in the NMR spectra, the solution is still viable for PCSD.

Table 1 Viscosity and surface tension at 23 °C in atmosphere for products and dilutions from proposed synthesis (Acac = acetylacetone; Bzac = benzoylacetone)

Solutions at 23 °C	Viscosity (mPa s)	Surface tension (mN m^{-1})
1,3-Propanediol	48.1	44
DEGEE	4.60	31
Acac product	347	45
40 wt% Acac prod.	15.4	34
30 wt% Acac prod.	10.3	33
Bzac product	850	45
30 wt% Bzac prod.	10.0	33

For the benzoylacetone based printed film, UV/Vis on a-SiO$_2$ in Fig. S19† shows an absorption peak at 348 nm before xenon flash lamp exposure, again demonstrating chelation of benzoylacetone to the tantalum cation.[42–44] More than 1000 shots are required for the chelation peak to diminish, and for a global maximum around 212 nm to form. Again, despite possible alcoholysis byproducts, the solution can be implemented in PCSD applications.

In the case of both the acetylacetone and benzoylacetone based films, the $\pi \rightarrow \pi$* transition metal ligand peaks are redshifted in comparison to the β-diketones' unbound form (319 nm in the film from $\sim$270 nm for acetylacetone, and 348 nm in the film from $\sim$310 nm for benzoylacetone),[73] which is to be expected.[41,43,44]

The remaining characterization results were only performed for the acetylacetone based films from the proposed synthesis method. This was done in order to avoid carbon impurities in the photocured oxide layer, as acetylacetone is a smaller molecule than benzoylacetone.

Raman and XRD – acetylacetone based film on a-SiO₂

The literature Raman spectra of Ta$_2$O$_5$ are very complex, containing multiple peaks which are dependent on whether the final compound is amorphous or crystalline.[74] The bands between 400 cm^{-1} and 900 cm^{-1} are associated with the coupled modes involving mainly the stretching and bending of the various Ta–O bonds. In the case of amorphous Ta$_2$O$_5$, the band at 670 cm^{-1} corresponds to the bending and stretching of triple-coordinated oxygen (O–3Ta) and the band at 800 cm^{-1} is due to the stretching of double-coordinated oxygen (O–2Ta).[22,74]

Fig. 4c shows the Raman spectra obtained from the thin tantalum oxide based layer on the a-SiO$_2$ substrate. These spectra were achieved after a hyperspectral analysis of the measured interface and subsequent subtraction of the remnant a-SiO$_2$ spectrum. Depth scans distinguishing the deposited and photocured tantalum oxide layer from the a-SiO$_2$ substrate are shown in Fig. S20,† where the thickness of the layer observed in the Raman image is thicker than the actual thickness; this is due to the lower *Z*-resolution in optical microscopy.

The lower spectrum (0 shots) in Fig. 4c was measured after a 125 °C thermal anneal, and the upper spectrum is of the same sample after 1000 flash lamp shots. Both spectra show a broad
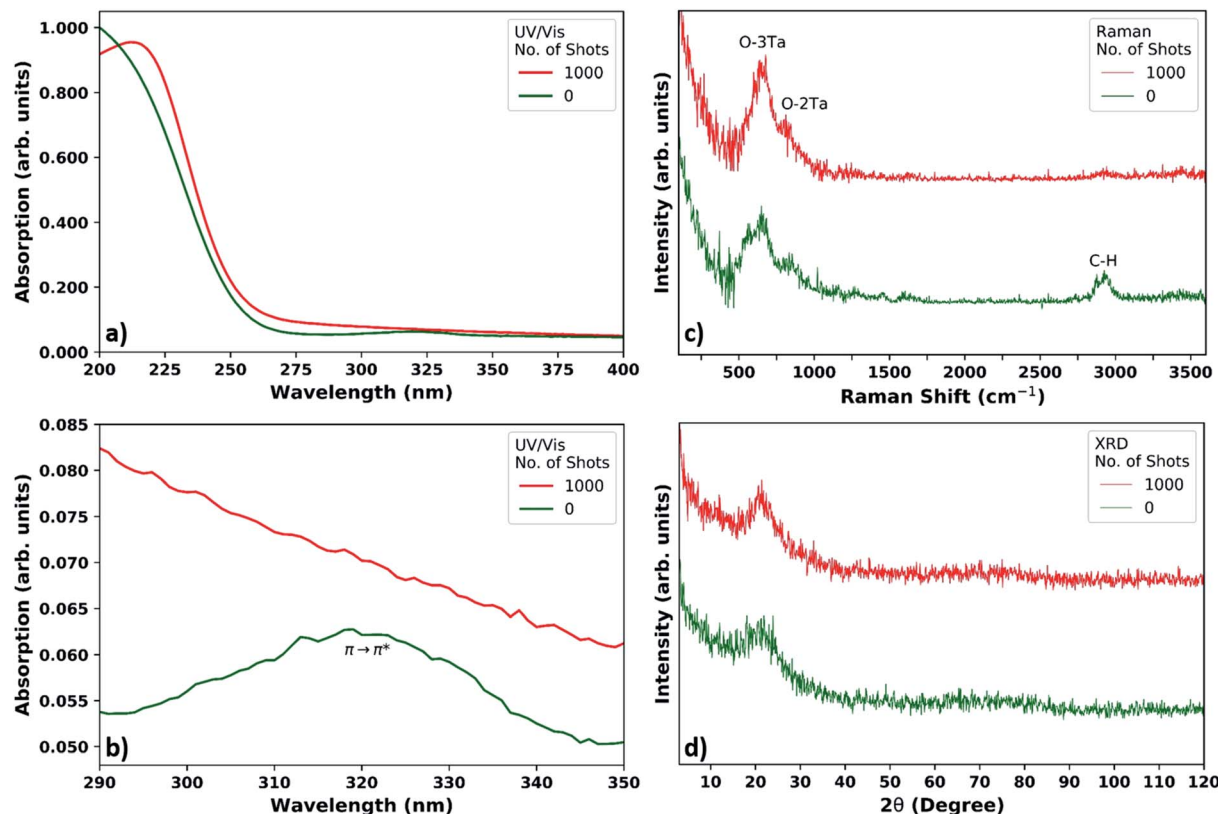
Fig. 4 UV/Vis spectra (a and b) of acetylacetone based layers on a-SiO$_2$, with (b) zooming in on the metal ligand absorption peak for the 0 shots sample. Raman (c) and XRD (d) appear to indicate that xenon flash lamp treatment may result in amorphous tantalum oxide films; UV/Vis spectra are normalized to the maximum of the 0 shots sample, while Raman and XRD spectra have been arbitrarily shifted for clarity.

peak around 670 cm^{-1} and a shoulder around 850 cm^{-1}, where these peaks correspond to amorphous Ta$_2$O$_5$.[22,74,75] X-ray diffraction (XRD) spectra in Fig. 4d supports inconclusively that photocuring at room temperature does not create crystalline Ta$_2$O$_5$, which is known to require temperatures above 600 °C.[18,74,75]

Before photocuring (0 shots), the Raman spectrum shows not only amorphous tantalum oxide peaks, but also organic peaks. These organic peaks are mainly observed around 2800 cm^{-1}, which corresponds to the C–H stretching modes of organic compounds. Additionally, the spectra of the precursors in Fig. S21† show that the precursor peaks are largely absent after photocuring.

RBS/NRA – acetylacetone based films on c-Si

The Rutherford backscattering spectrometry (RBS) and nuclear reaction analysis (NRA) spectra of the 125 °C pre-annealed samples show sharp peak forms in Fig. 5a and b (0 shots and 1000 shots, respectively), and correspondingly all detected material lies in the first resolution bin of 5.5 × 10^{21} atoms per m^2. The quantitative data is tabulated in Table 2, and the layer thicknesses are in the range of 1.0 × 10^{21} atoms per m^2 to 1.5 × 10^{21} atoms per m^2. Small amounts of carbon corresponding to a few atom% (at%) in the layer were found in both samples. The oxygen to tantalum ratios in the 1000 shots sample do not

match the Ta$_2$O$_5$ stoichiometry within error, with an oxygen excess of O/Ta = 3.9 ± 0.5 (ideally O/Ta = 2.5) and exceeding that of anodic tantalum oxide NRA oxygen standards.[76–78] The extra oxygen could be due to SiO$_2$ formation, organics, or water. Due to the limited depth-resolution, it cannot be excluded that some of the oxygen is present near the surface of or in the c-Si substrate. Although the layer thicknesses vary, the O/Ta ratio stays constant within uncertainties.

The carbon content of the printed layers appears to decrease after flash lamp annealing, and the ^{12}C(d,p$_0$)^{13}C peak decreases from the 0 shots to the 1000 shots samples relative to the ^{16}O(d,p$_0$)^{17}O peak. The amount of detected carbon would correspond to a few monolayers of graphite; however, surface contamination may influence the presence of carbon.

XPS – acetylacetone based films on Au/Ti/PET

X-ray photoelectron spectroscopy (XPS) survey spectra of the samples are shown in Fig. S22 and S23† for the 0 shots and 1000 shots samples (both with 125 °C pre-anneal), respectively. The carbon content of the printed layers appears to decrease after flash lamp annealing, as shown in Table 3. However, the presence of carbon is also influenced by surface contamination, and therefore may not be an accurate indicator of layer carbon content. Nonetheless, xenon flash lamp treatment appears to reduce the amount of carbon present on the samples.
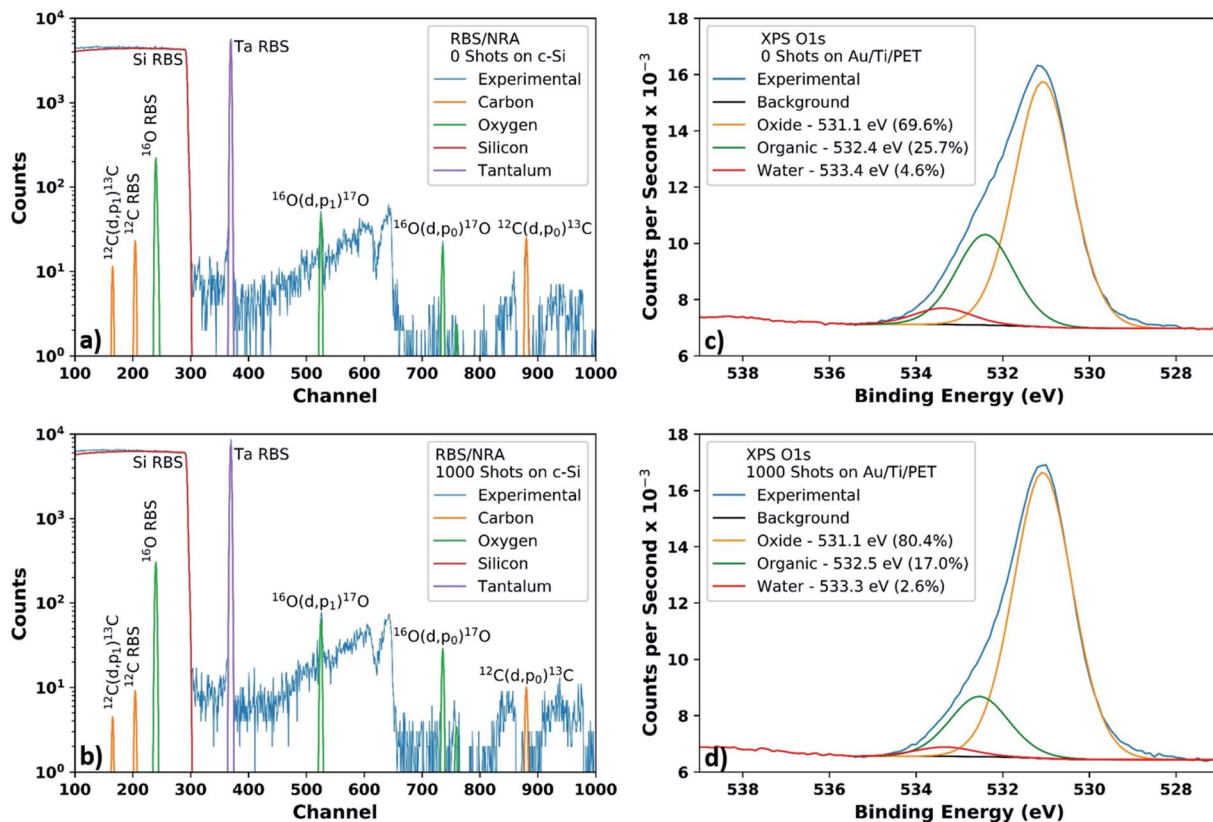
Fig. 5 RBS/NRA spectra of samples on c-Si for 0 shots (a) and 1000 shots (b) with simulated element peaks superimposed on the experimental data – the $^{12}C(d,p_0)^{13}C$ peak appears to decrease relative to the $^{16}O(d,p_0)^{17}O$ peak after xenon flash lamp exposure; XPS O 1s spectra of samples on Au/Ti/PET foil for 0 shots (c) and 1000 shots (d) – the organic peak appears to decrease after xenon flash lamp exposure.

Table 2 Atom content (10 at% relative uncertainty due to the counting statistics of ^{16}O NRA, assuming homogenous layer) from RBS and NRA analysis, with layer thickness in 10^{19} at. per m^2, c-Si wafer

Sample	at% C	at% O	at% Ta	Thickness
(1) 0 shots	10.9	70.7	18.4	149
(2) 1000 shots	3.3	76.7	19.9	143

On both the 0 shots and the 1000 shots samples, the binding energies at 26.8 eV for Ta $4f_{7/2}$ (57.1% Ta 4f area) and 28.7 eV for Ta $4f_{5/2}$ (42.9% Ta 4f area) are present, indicating the presence of one oxidation state which does not change after photocuring. This oxidation state would be +5 for Ta_2O_5.[79] Ta 4f spectra for both samples can be seen in Fig. S24,† along with the C 1s spectra with fitted peaks.[80] Although the detected ester groups

Table 3 Atom content (15 at% relative uncertainty, assuming homogenous layer) via XPS of layers printed on wet-etched Au/Ti/PET foil. XPS data are more surface sensitive than RBS/NRA data, which may account for the large differences in at%

Sample	at% C 1s	at% O 1s	at% Ta 4f	at% Au 4f
(1) 0 shots	40.9	47.9	10.7	0.4
(2) 1000 shots	16.5	64.2	17.4	1.9

could come from acetylated 1,3-propanediol, the presence of esters could also be due to organic contaminants.

For the O 1s binding energies in Fig. 5c for 0 shots and Fig. 5d for 1000 shots, an increase in oxide oxygen and a decrease in organic oxygen is visible after photocuring.[81] The O/Ta oxide ratio in the 1000 shot sample is 3.0, showing an excess of oxygen like the RBS/NRA samples. However, there is a difficult to ascertain error from the overlapping integrals. Furthermore, as XPS is a surface characterization method, there could be different amounts of oxygen on the surface and in the bulk, which would also affect the O/Ta ratio.

LCR meter – acetylacetone based films on Au/Ti/PET foil

After deposition and 125 °C annealing on wet-etched, inter-digitated structures, parallel capacitance increases and parallel resistance decreases with exposure to a xenon flash lamp, as shown in Fig. 6a. After about 500 shots, the parallel capacitance levels off at just over 80 pF, and the parallel resistance at roughly 200 kΩ. The leakage current could be due either to carbon impurities,[42,82–84] or oxygen vacancies and other defects.[40]

Elucidation of the exact leakage current mechanism would require an improved model, such as using a metal–insulator–metal (MIM) configuration and an impedance analyser.[72] However, given that the oxide layer needs to be exposed for pho-tocuring, such a configuration would prove challenging. One
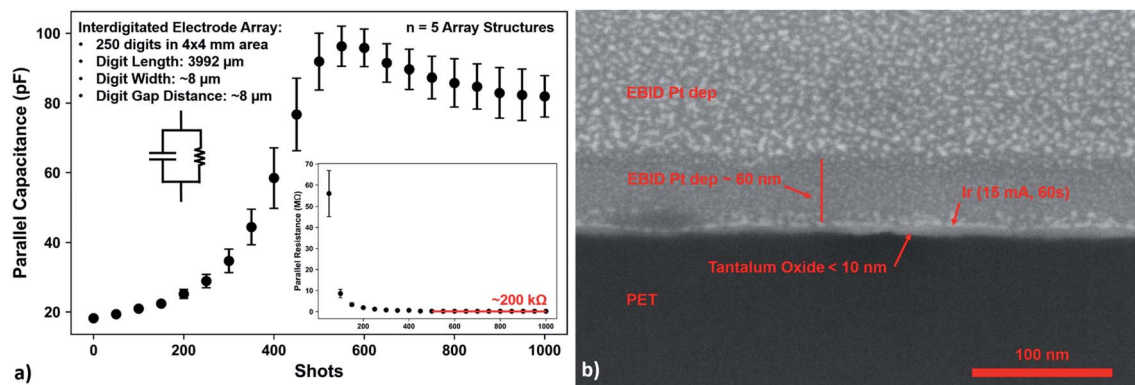
Fig. 6 LCR meter measurements (a) of wet-etched, interdigitated gold structures on PET foil. The parallel capacitance appears to peak after 500 shots, and the parallel resistance levels off at roughly 200 kΩ. FIB sectioning and SEM (b) after a total of 5000 shots and a 2 hour 125 °C post-anneal shows a resulting tantalum oxide layer between the gold fingers being less than 10 nm thick (image: 1 000 000×, 52° tilt).

solution to this problem in future studies could be to produce many MIM samples while following the procedure of Matavž et al.,[72] with each sample having a different amount of photo-exposure. Furthermore, the layer geometry would need to be defect free and accurately ascertained for the model. Additionally, the layer thickness could affect the diffusion of carbon volatiles leaving the layer, as well as oxygen diffusion in filling oxygen vacancies in the layer.

FIB/SEM – acetylacetone based films on Au/Ti/PET foil

The printed films on Au/Ti/PET foils were further exposed to 4000 more flash lamp shots, in order to be sure the photosensitive compounds were destroyed. The foils were then exposed to another 125°C post-anneal (1 hour ramp, 2 hour hold) to condense the films, whereby FIB sectioning and SEM in Fig. 6b reveal a tantalum oxide layer between the gold fingers which is less than 10 nm thick. Such an oxide film deposited on interdigitated, gold structures could potentially be used in pH or conductivity sensors.[10,13]

Conclusions

A method to reduce alcoholysis for photosensitive tantalum(v) β-diketonate complexes in an air stable, low-toxic solution is presented. Inkjet printed oxide layers produced from the solution after xenon flash lamp curing shows that the photosensitive complexes break down and that the carbon content is reduced to form tantalum oxide films, which potentially could be used in various applications. Electrical characterization demonstrates that the capacitance and the conductivity of the layers change after photocuring on interdigitated electrodes, which we believe will inspire further research on metal oxide films deposited in this manner.

Experimental

Proposed synthesis – acetylacetone

Anhydrous ethanol (42.33 mmol, 1950 mg [AcrosOrganics, 99.5%, ExtraDry, absolute]), acetylacetone (6.15 mmol, 616 mg, [Alfa-Aesar,

95%]), and tantalum(v) ethoxide (6.15 mmol, 2499 mg [Alfa Aesar, 99+%]) were mixed together *via* magnetic stirring in a dry Schlenk flask in an argon filled glovebox, and were subsequently removed from the glovebox and connected to a Schlenk line. The Schlenk flask containing the reagents (reaction flask) was immersed in silicone oil, with the oil temperature being held and maintained at 80 °C to promote chelation of acetylacetone. The reaction was carried out in argon, and reflux was conducted for 8 hours with mixing to allow enough time for complexation of acetylacetone to tantalum;[48,55,63] the reaction time was minimized as much as possible in order to prevent decomposition of the complex.[59]

After 8 hours, the flask was cooled to 23 °C over a 2 hour period. 1,3-Propanediol (42.04 mmol, 3199 mg [Sigma-Aldrich, for synthesis]) was then added *via* syringe through the Schlenk flask valve and mixed, where bubbles appeared for a short time but eventually disappeared. After 12 hours of mixing at a reduced temperature, the Schlenk flask was removed from the Schlenk line. The product was subsequently transferred from the Schlenk flask to a round bottom flask, and the round bottom flask was then connected to a rotary evaporator. The rotation speed was set to 95 rpm, the pressure was set to 30 mbar, and the water bath temperature was set to 40 °C. Vigorous bubbling was present at the beginning, but the bubbling eventually dissipated. The flask remained attached for 8 hours, where afterward it was found that the mass loss (3236 mg) was close to the calculated ethanol loss (3367 mg). The product was prepared for NMR, but not enough distillate could be collected for NMR analysis.

Proposed synthesis – benzoylacetone

The synthesis is the same as that proposed for acetylacetone, except with the following reagent quantities: anhydrous ethanol (54.24 mmol, 2499 mg [AcrosOrganics, 99.5%, ExtraDry, absolute]), benzoylacetone (5.99 mmol, 972 mg [Sigma-Alrich, 99%]), tantalum(v) ethoxide (6.12 mmol, 2486 mg [Alfa Aesar, 99+%]), and 1,3-propanediol (42.16 mmol, 3208 mg [Sigma-Aldrich, for synthesis]). For ethanol removal, the mass loss (3681 mg) was close to the calculated ethanol loss (3909 mg). The product was prepared for NMR, but not enough distillate could be collected for NMR analysis.

NMR measurements

All NMR spectra were recorded at 25 °C using a 600 MHz AVANCE NMR spectrometer (Bruker Corporation, USA). Chemical shifts for the reagents and products are relative to the residual proton signal of the external deuterated solvent, D_2O, used as a reference; one exception is benzoylacetone, which was dissolved in a $CDCl_3$ reference solvent.

Inkjet printing and photonic curing

Dilutions for ink production from the proposed methods were performed by vortexing the product with diethylene glycol monoethyl ether (DEGEE) (Sigma-Aldrich, ReagentPlus 99%) in order to achieve the proper viscosity and surface tension for inkjet printing.[72] Viscosity was measured with a DV3T rheometer (AMETEK Brookfield, USA), and surface tension with a surface tensiometer model A3 (KINO Industry Co., Ltd., USA). All inkjet printing was performed with an OmniJet 300 printer (Unijet Co., Ltd., South Korea), using 10 pL Dimatix cartridges (FUJIFILM Dimatix, Inc., USA) where the ink was filtered using a Whatman Puradisc 13, GF/F, 0.7 μm glass syringe filter (GE Healthcare, USA). The printing waveform was set to 1 μs–10 μs–1 μs at 25 V, with a frequency of 1000 Hz.

After deposition, all samples were treated with thermal annealing, which entailed a 1 hour ramp to 125 °C and a 2 hour hold on a hot plate. This was followed by xenon flash lamp exposure for photocured samples, which was carried out with the PulseForge 1200 (Novacentrix, USA) with an output spectrum from roughly 230 nm–1000 nm at the set voltage.[84] Multiple, low power "shots" were utilized in order to protect the fragile gold foil structures for electrical characterization (described below), with each shot having the following parameters: 400 V, 900 μs envelope containing 3 pulses with a 100 μs rise time and a 200 μs fall time, with a firing frequency of 0.33 Hz and a working distance of 25 mm. The estimated energy for each shot was 0.623 J cm^{-2}. The SimPulse 2.5 software provided by the manufacturer estimates a plateau in surface temperature during the 1000 shot treatment at 0.33 Hz and an operating temperature of 25 °C: 500 μm thick a-SiO_2, ~25 °C; 500 μm thick c-Si ~60 °C; 80 μm thick PET, ~25 °C; 80 μm thick PET with 5 nm Ti adhesion layer and 50 nm Au layer, ~300 °C.

Deposition on a-SiO_2 for UV/Vis spectrophotometry

0.5 mm thick a-SiO_2 was chosen as the best substrate for transparency in the near UV range. Before printing, the substrate was subjected to an oxygen plasma treatment for 5 minutes (120 W, 0.6 mbar) using the NANO plasma oven (Diener electronic GmbH + Co. KG, Germany).

Product from the proposed method with acetylacetone was diluted with DEGEE, with the dilution containing 706 mg of DEGEE (70 wt%) and 308 mg of product (30 wt%). The ink was then printed on the substrate with a 150 μm drop pitch having dimensions of 250 × 120 drops to create a uniform layer.

For benzoylacetone, the dilution contained 732 mg DEGEE (69 wt%) and 328 mg of product (31 wt%). The ink was then printed with a smaller drop pitch of 75 μm to create uniform layers (the benzoylacetone ink did not spread as well as the acetylacetone ink), having dimensions of 400 × 220 drops to create a uniform layer.

UV/Vis spectrophotometry

UV/Vis spectra of the films on a-SiO_2 were measured *versus* a 0.5 mm thick a-SiO_2 reference, with a 1 nm step in the 200 nm to 400 nm range. The device used was a Lambda 900 spectrometer (PerkinElmer, USA).

Deposition on a-SiO_2 for Raman/XRD

a-SiO_2 was used to avoid interfering peaks in both Raman spectroscopy and X-ray diffraction (XRD) measurements. Before printing, the substrate was subjected to an oxygen plasma treatment for 5 minutes (150 W, 0.6 mbar). The power was set slightly higher to increase spreading as the ink contained less DEGEE.

Product from the proposed method with acetylacetone was diluted with DEGEE, with the dilution containing 611 mg of DEGEE (60 wt%) and 404 mg of product (40 wt%). The ink was then printed on 0.5 mm thick a-SiO_2, with a 70 μm drop pitch having dimensions of 450 × 275 drops to create a uniform layer. The ink was printed with a smaller pitch and diluted with less DEGEE than for the UV/Vis samples, in order to obtain higher quality Raman spectra.

Raman spectroscopy

Confocal Raman microscopy was performed using an alpha300 R setup (WITec, Germany). Illumination of the sample was performed using a 532 nm excitation line from a single-mode frequency doubled Nd:YAG laser *via* a 100 μm single-mode glass fiber. A LD EC Epiplan-Neofluar 50×/0.55 objective (Carl Zeiss AG, Germany) was used and the laser power at the sample behind the objective was 12 mW.

An edge filter was used to separate the Raman signal from the excitation line. Confocality of the Raman signal was achieved *via* a 50 μm multi-mode fiber glass between the microscope and the Raman spectrometer, where the fiber serves as a pin-hole. The Raman spectrometer was equipped with a holographic grating of 600 lines per mm. For the detector, a Newton 970 EMCCD camera (Andor Technology Ltd, United Kingdom) with 1600 × 200 pixels was used, where this configuration allows a spectral resolution of about 2 cm^{-1} to be obtained.

An integration time of roughly 0.1 s per spectrum and pixel was used to improve the signal-to-noise ratio (S/N). For Raman depth scans, 100 pixel × 80 pixel scans were used for covering an area of 50 μm × 40 μm. All data sets were analyzed using cluster analysis and non-negative matrix factorization.

XRD

X-ray measurements were accomplished with a high-resolution D8 diffractometer (Bruker Corporation, USA), using the CuKα1 wavelength ($\lambda = 1.54016$ Å) collimated and filtered by means of a Göbel mirror and a Ge-220 four-crystal monochromator. On

the detector side, a scintillator with a mechanical slit of 3 mm was employed. The $2\theta/\theta$ scans were carried out in a range from $2\theta = 3–120°$ with angular resolutions of 0.1°. Each data point was measured for 10 s.

Deposition on c-Si for RBS/NRA

The ink was deposited on c-Si in order to determine whether PCSD is possible on this standard substrate, and used Rutherford backscattering spectrometry (RBS) and nuclear reaction analysis (NRA) to measure tantalum, carbon, and oxygen content after treatment. Before printing, the substrate was subjected to an argon plasma treatment for 5 minutes (150 W, 0.6 mbar).

Product from the proposed method with acetylacetone was diluted with DEGEE, with the dilution containing 622 mg of DEGEE (60 wt%) and 414 mg of product (40 wt%). The ink was then printed on 0.5 mm thick c-Si, with a 70 μm drop pitch having dimensions of 75 × 75 drops to create a uniform layer.

RBS/NRA

RBS and NRA were performed using 1.43 MeV deuterons. A beam spot diameter of about 200 μm was set up using a triple-focus. A 20 μm resolution imaging camera together with a piezo manipulator enabled positioning of the beam spot on the regions of interest on each sample. Each sample spot was integrated for about 2000 s to about 3 μC of ion charge for sufficient counting statistics. Signals were acquired using a 100 μm thick PIPS detector with 11 keV FWHM resolution at 150° reaction angle.

RBS and NRA data were analysed using SimNRA 7.02 with Rutherford cross-sections for all elements except for C and O which were analyzed using $^{16}O(d,p_0)^{17}O$ and the $^{12}C(d,p_0)^{13}C$ reactions and Sigmacalc 2.0 cross-sections. The measurement achieves a total uncertainty of 10% originating from the Particle*Sr value determined from the substrate RBS and NRA counting statistics. The good counting statistics of tantalum results in negligible uncertainties for this element.

Deposition on gold foil for XPS and LCR meter measurements

The ink was deposited on gold/titanium/PET foil (metallization via electron-beam physical vapor deposition of less than 50 nm of gold with ~5 nm titanium as adhesion layer on 80 μm DuPont PCS) to see if the ink could be cured on a low melting point substrate. The gold foils also allowed for electrical characterization and for higher quality X-ray photoelectron spectroscopy (XPS) spectra, which were wet-etched to create interdigitated structures consisting of 250 digits in a 4 mm × 4 mm area (digit length of ~3992 μm, width and gap length of ~8 μm); the structures were connected to feedlines to allow for LCR meter measurements. Before printing, the substrate was subjected to an oxygen plasma treatment for 2 minutes (150 W, 0.6 mbar).

Product from the proposed method with acetylacetone was diluted with DEGEE, with the dilution containing 622 mg of DEGEE (60 wt%) and 414 mg of product (40 wt%). The ink was then printed on the gold PET foil with interdigitated structures,

with a 150 μm drop pitch having dimensions of 35 × 31 drops to create a uniform layer.

XPS

Spectra were obtained using a Phi5000 VersaProbe II (ULVAC-Phi Inc., USA). The source was AlKα, monochromatic (1.486 keV) with X-ray settings of 50 W, 15 kV in a 200 μm spot. Survey spectra were obtained with a 187.5 eV pass energy, with a 0.8 eV step and 100 ms per step. Detailed spectra used a 23.5 eV pass energy, with a 0.1 eV step and 100 ms per step.

Atomic quantification assumed a homogenous volume, using atomic% (at%) with a 15% relative error. Quantification was normalized to 100 at%. The Shirley-background was subtracted and empirical relative sensitivity factors were used. Charge compensation was performed by setting the main peak of the C 1s signal to 285 eV.

LCR meter measurements

After the 125 °C preliminary anneal, the layers were exposed to the xenon flash lamp, with the parallel capacitance (with parasitic capacitance subtracted) and the parallel resistance measured at 1000 Hz every 50 shots, using a DE-5000 LCR meter with TL-22 probes (DER-EE, Taiwan). Plotted values were an average from 5 structures, with the error bar reporting the standard deviation.

FIB and SEM

Focused ion beam (FIB) sectioning and subsequent scanning electron microscopy (SEM) imaging was carried out with a HELIOS 600i NanoLab (FEI, Thermo Fisher Scientific, USA). First the region of interest on the sample was covered in situ with protective Pt/C layers. Rough milling was processed with Ga^+ ions at 0.43 or 0.79 nA and 30 kV followed by a fine polishing step at 40 pA and 30 kV. SEM imaging was performed at 21 pA and 3 kV using the TL detector for secondary electrons.

Conflicts of interest

We declare that Christopher Beale, Stefanie Hamacher, Dirk Mayer, and Andreas Offenhäusser have filed a German patent application (Date: Oct 08, 2019; application number: DE 10 2019 006 976.5) on behalf of Forschungszentrum Jülich GmbH. The patent application includes the synthesis methods and their products described in this publication, with the intended use being the deposition of metal oxide material. All other authors have no conflicts to declare.

Acknowledgements

for the project "EFRE-0800361 Packsense", was used for this study.

References

1 O. H. Fulcher, *J. Am. Med. Assoc.*, 1943, **121**, 931.

2 G. L. Burke, *Can. Med. Assoc. J.*, 1940, **43**, 125–128.

3 D. Fraser, G. Mendonca, E. Sartori, P. Funkenbusch, C. Ercoli and L. Meirelles, *Clin. Oral Implants Res.*, 2019, **30**, 156–168.

4 M. Papakyriacou, *Int. J. Fatigue*, 2000, **22**, 873–886.

5 Y. Freeman, *Tantalum and Niobium-Based Capacitors*, Springer International Publishing, Cham, 2018.

6 J. Ma, X. Guo, H. Xue, K. Pan, C. Liu and H. Pang, *Chem. Eng. J.*, 2020, **380**, 122428.

7 S. Uhlenbruck, J. Dornseiffer, S. Lobe, C. Dellen, C.-L. Tsai, B. Gotzen, D. Sebold, M. Finsterbusch and O. Guillon, *J. Electroceram.*, 2017, **38**, 197–206.

8 N. Özer and C. M. Lampert, *Windows Innovations 95 Conference Proceedings*, Berkeley Laboratory, Livermore, 1995, LBL-38526, https://windows.lbl.gov/publications/sol-gel-deposited-amorphous-tantalum-oxide-and-niobium-oxide-films-protonic-conductors.

9 R. E. G. van Hal, J. C. T. Eijkel and P. Bergveld, *Sens. Actuators, B*, 1995, **24**, 201–205.

10 W. Olthuis, W. Streekstra and P. Bergveld, *Sens. Actuators, B*, 1995, **24**, 252–256.

11 M. J. Schöning, D. Brinkmann, D. Rolka, C. Demuth and A. Poghossian, *Sens. Actuators, B*, 2005, **111–112**, 423–429.

12 C. H. Kao, H. Chen, L. T. Kuo, J. C. Wang, Y. T. Chen, Y. C. Chu, C. Y. Chen, C. S. Lai, S. W. Chang and C. W. Chang, *Sens. Actuators, B*, 2014, **194**, 419–426.

13 L. Manjakkal, B. Cvejin, B. Bajac, J. Kulawik, K. Zaraska and D. Szwagierczak, *Electroanalysis*, 2015, **27**, 770–781.

14 M. Biednov, T. Lebyedyeva and P. Shpylovyy, *Proc. of SPIE Optical Sensors*, 2015, vol. 9506, pp. 95061P.

15 D. Li, W. Zhang, H. Liu, J. Hu and G. Zhou, *IEEE Photonics J.*, 2017, **9**, 1–8.

16 M. R. Hasan, S. Akter, K. Ahmed and D. Abbott, *IEEE Photonics Technol. Lett.*, 2018, **30**, 315–318.

17 A. González García, *Láminas delgadas y ultradelgadas de tantalato de estroncio y bismuto obtenidas a partir de derivados de glicolato de tántalo para su uso en memorias ferroeléctricas no volátiles*, PhD thesis, Autonomous University of Madrid, Spain, November 2002.

18 M. L. Calzada and A. González, *J. Am. Ceram. Soc.*, 2005, **88**, 2702–2708.

19 M. L. Calzada, M. Algueró, J. Ricote, A. Santos and L. Pardo, *J. Sol-Gel Sci. Technol.*, 2007, **42**, 331–336.

20 M. L. Calzada, M. Algueró, A. Santos, M. Stewart, M. G. Cain and L. Pardo, *J. Mater. Res.*, 2009, **24**, 526–533.

21 M. D. Anderson, B. Aitchison and D. C. Johnson, *ACS Appl. Mater. Interfaces*, 2016, **8**, 30644–30648.

22 T. Damart, E. Coillet, A. Tanguy and D. Rodney, *J. Appl. Phys.*, 2016, **119**, 175106.

23 N. A. Mancheri, B. Sprecher, S. Deetman, S. B. Young, R. Bleischwitz, L. Dong, R. Kleijn and A. Tukker, *Resour., Conserv. Recycl.*, 2018, **129**, 56–69.

24 T. Nakajima, K. Shinoda and T. Tsuchiya, *Chem. Soc. Rev.*, 2014, **43**, 2027–2041.

25 A. Matavž and B. Malič, *J. Sol-Gel Sci. Technol.*, 2018, **87**, 1–21.

26 I. Bretos, R. Jiménez, J. Ricote and M. L. Calzada, *Chem. Soc. Rev.*, 2018, **47**, 291–308.

27 D. Grosso, C. Boissière and M. Faustini, in *The Sol-Gel Handbook*, Wiley-VCH Verlag GmbH & Co. KGaA, Weinheim, Germany, 2015, pp. 277–316.

28 M. L. Calzada, in *The Sol-Gel Handbook*, ed. D. Levy and M. Zayat, Wiley-VCH Verlag GmbH & Co. KGaA, Weinheim, Germany, 2015, pp. 841–882.

29 R. Deshmukh and M. Niederberger, in *The Sol-Gel Handbook*, Wiley-VCH Verlag GmbH & Co. KGaA, Weinheim, Germany, 2015, p. 34.

30 G. A. Seisenbaeva and V. G. Kessler, *Nanoscale*, 2014, **6**, 6229–6244.

31 H. C. Ling, M. F. Yan and W. W. Rhodes, in *Science of Ceramic Chemical Processing*, ed. L. L. Hench and D. R. Ulrich, John Wiley & Sons, Inc., New York, 1986, pp. 285–303.

32 L. A. Silverman, G. Teowee and D. R. Uhlmann, *MRS Proceedings*, 1986, **72**, 331.

33 L. A. Silverman, Sol-gel derived tantalum oxide thin films, PhD thesis, Massachusetts Institute of Technology, United States, June 1987.

34 P. Griesmar, G. Papin, C. Sanchez and J. Livage, *Chem. Mater.*, 1991, **3**, 335–339.

35 I. Bretos and M. L. Calzada, in *Multifunctional Polycrystalline Ferroelectric Materials - Processing and Properties*, ed. L. Pardo and J. Ricote, Springer, Dordrecht, 2011, vol. 152–155, pp. 182–186.

36 J. F. Scott, in *Ferroelectric Memories*, Springer-Verlag, Berlin, 2000, p. 166.

37 R. C. Mehrotra and P. N. Kapoor, *J. Less-Common Met.*, 1965, **8**, 419–427.

38 R. C. Mehrotra and P. N. Kapoor, *J. Less-Common Met.*, 1965, **10**, 237–245.

39 T. Ohishi, S. Maekawa and A. Katoh, *J. Non-Cryst. Solids*, 1992, **147–148**, 493–498.

40 I. W. Boyd and J.-Y. Zhang, *Solid-State Electron.*, 2001, **45**, 1413–1431.

41 N. Tohge, K. Shinmou and T. Minami, *J. Sol-Gel Sci. Technol.*, 1994, **2**, 581–585.

42 K. Suzuki, W. Sakamoto, T. Yogo and S. Hirano, *J. Ceram. Soc. Jpn.*, 1999, **107**, 1032–1036.

43 T. H. Park, K. H. Yang, D. K. Kang, T. Y. Lim, K. H. Auh and B. H. Kim, *J. Mater. Sci.*, 2003, **38**, 1295–1300.

44 T. Y. Lim, K. H. Yang, B. H. Kim and K. H. Auh, *Thin Solid Films*, 2005, **471**, 12–18.

45 N. Noma and M. Hamano, *J. Sol-Gel Sci. Technol.*, 2012, **64**, 297–303.

46 H. Segawa, S. Inoue, K. Watanabe, R. Ohashi, H. Nitani and M. Nomura, *J. Ceram. Soc. Jpn.*, 2015, **123**, 793–799.

47 R. J. Squibb, M. Sapunar, A. Ponzi, R. Richter, A. Kivimäki, O. Plekan, P. Finetti, N. Sisourat, V. Zhaunerchyk, T. Marchenko, L. Journel, R. Guillemin, R. Cucini, M. Coreno, C. Grazioli, M. Di Fraia, C. Callegari, K. C. Prince, P. Decleva, M. Simon, J. H. D. Eland,

N. Došlić, R. Feifel and M. N. Piancastelli, *Nat. Commun.*, 2018, **9**, 1–7.

48 A. Whitley, New metal alkoxides, PhD thesis, Birkbeck College, University of London, United Kingdom, November 1954.

49 D. C. Bradley, W. Wardlaw and A. Whitley, *J. Chem. Soc.*, 1955, 726–728.

50 H. Funk and K. Niederländer, *Ber. Dtsch. Chem. Ges.*, 1929, **62**, 1688–1691.

51 H. Funk, *Ber. Dtsch. Chem. Ges.*, 1934, **67**, 1801–1804.

52 D. C. Bradley, R. C. Mehrotra, I. P. Rothwell and A. Singh, in *Alkoxo and Aryloxo Derivatives of Metals*, Academic Press, London, 2001, vol. 121.

53 R. C. Mehrotra and P. N. Kapoor, *J. Less-Common Met.*, 1964, **7**, 453–457.

54 R. C. Mehrotra and P. N. Kapoor, *J. Less-Common Met.*, 1964, **7**, 176–179.

55 P. N. Kapoor and R. C. Mehrotra, *J. Less-Common Met.*, 1965, **8**, 339–346.

56 R. N. Kapoor, S. Prakash and P. N. Kapoor, *Bull. Chem. Soc. Jpn.*, 1967, **40**, 1384–1386.

57 M. L. Calzada, R. Sirera, F. Carmona and B. Jiménez, *J. Am. Ceram. Soc.*, 1995, **78**, 1802–1808.

58 M. L. Calzada, A. González, R. Poyato and L. Pardo, *J. Mater. Chem.*, 2003, **13**, 1451–1457.

59 T. Kemmitt and M. Daglish, *Inorg. Chem.*, 1998, **37**, 2063–2065.

60 G. Ambrožič, S. D. Škapin, M. Žigon and Z. C. Orel, *J. Colloid Interface Sci.*, 2010, **346**, 317–323.

61 M. Staniuk, D. Zindel, W. van Beek, O. Hirsch, N. Kränzlin, M. Niederberger and D. Koziej, *CrystEngComm*, 2015, **17**, 6962–6971.

62 R. K. Sodhi and S. Paul, *Catal. Surv. Asia*, 2018, **22**, 31–62.

63 K. D. Pollard and R. J. Puddephatt, *Chem. Mater.*, 1999, **11**, 1069–1074.

64 D. Ambrose and C. H. S. Sprake, *J. Chem. Thermodyn.*, 1970, **2**, 631–645.

65 "Ethanol" National Institute of Standards and Technology Chemistry WebBook, United States Department of Commerce, 2018.

66 D. R. Stull, *Ind. Eng. Chem.*, 1947, **39**, 517–540.

67 "1,3-propanediol," National Institute of Standards and Technology Chemistry WebBook, United States Department of Commerce, 2018.

68 S. S. Likhodii and W. M. Burnham, *Med. Sci. Monit.*, 2002, **8**, HY19–HY24.

69 J. B. Lambert, E. P. Mazzola and C. D. Ridge, *Nuclear Magnetic Resonance Spectroscopy: An Introduction to Principles, Applications, and Experimental Methods*, John Wiley & Sons, Inc., Hoboken, 2nd edn, 2019, vol. 86, p. 99.

70 Y. Zhao, J. Q. L. Ang, A. W. T. Ng and Y.-Y. Yeung, *RSC Adv.*, 2013, **3**, 19765.

71 Y. Takebayashi, S. Yoda, T. Sugeta, K. Otake, T. Sako and M. Nakahara, *J. Chem. Phys.*, 2004, **120**, 6100–6110.

72 A. Matavž, R. C. Frunza, A. Drnovšek, V. Bobnar and B. Malič, *J. Mater. Chem. C*, 2016, **4**, 5634–5641.

73 P. K. Verma, A. Steinbacher, F. Koch, P. Nuernberger and T. Brixner, *Phys. Chem. Chem. Phys.*, 2015, **17**, 8459–8466.

74 C. Joseph, P. Bourson and M. D. Fontana, *J. Raman Spectrosc.*, 2012, **43**, 1146–1150.

75 Y. Zhu, F. Yu, Y. Man, Q. Tian, Y. He and N. Wu, *J. Solid State Chem.*, 2005, **178**, 224–229.

76 G. Amsel, J. P. Nadai, C. Ortega, S. Rigo and J. Siejka, *Nucl. Instrum. Methods*, 1978, **149**, 705–712.

77 G. Amsel, J. P. Nadai, C. Ortega and J. Siejka, *Nucl. Instrum. Methods*, 1978, **149**, 713–720.

78 G. Amsel and J. A. Davies, *Nucl. Instrum. Methods Phys. Res.*, 1983, **218**, 177–182.

79 R. Simpson, R. G. White, J. F. Watts and M. A. Baker, *Appl. Surf. Sci.*, 2017, **405**, 79–87.

80 J.-H. Zhou, Z.-J. Sui, J. Zhu, P. Li, D. Chen, Y.-C. Dai and W.-K. Yuan, *Carbon*, 2007, **45**, 785–796.

81 L. Chen and R. W. Hoffman, *J. Vac. Sci. Technol., A*, 1993, **11**, 2303–2307.

82 K. Tetzner, K. A. Schroder and K. Bock, *Ceram. Int.*, 2014, **40**, 15753–15761.

83 K. Tetzner, Y. H. Lin, A. Regoutz, A. Seitkhan, D. J. Payne and T. D. Anthopoulos, *J. Mater. Chem. C*, 2017, **5**, 11724–11732.

84 S. Luo, S. Zhang, B. B. Bourgeois, B. C. Riggs, K. A. Schroder, Y. Zhang, J. He, S. Adireddy, K. Sun, J. T. Shipman, M. M. Oguntoye, V. Puli, W. Liu, R. Tu, L. Zhang, S. Farnsworth and D. B. Chrisey, *J. Mater. Res.*, 2017, **32**, 1701–1709.